



Firmly combination of CoMnO_x nanocrystals supported on N-doped CNT for lithium-ion batteries



Yuankun Wang, Shujing Wang, Tingting Zhao, Yan Chen, Zhongtao Li^{*}, Wenting Wu, Mingbo Wu^{*}

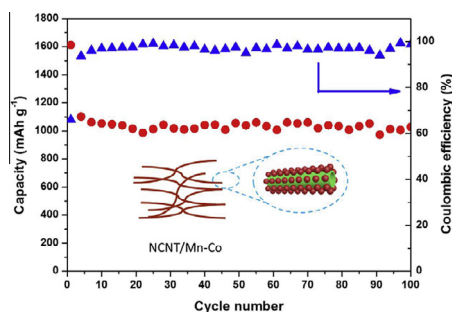
State Key Laboratory of Heavy Oil Processing, School of Chemical Engineering, China University of Petroleum, Qingdao 266580, China

HIGHLIGHTS

- One-step synthesis of Mn-Co/N-CNT has been proposed for the first time.
- Dicyandiamide act as surfactant and N source during Mn-Co deposition process.
- N-doping helps to improve the interaction between Mn-Co species and CNT.
- The Mn-Co/N-CNT shows high reversible capacity and good stability.

GRAPHICAL ABSTRACT

A novel one-dimensional Mn-Co/N-CNT composite was readily synthesized by in situ banding Mn-Co nanoparticles on nitrogen doped carbon nanotubes (N-CNT) through solvothermal method and followed by high temperature pyrolysis. The as-made Mn-Co/N-CNT as LIBs anode material exhibits excellent rechargeable capability, i.e. $1028 \text{ mAh}\cdot\text{g}^{-1}$ at $200 \text{ mA}\cdot\text{g}^{-1}$. Doped nitrogen on CNT effectively increase the conductivity of the complex and the binding energy between Mn-Co nanoparticles and CNT, which lead to more stable and higher conductive complex during charge/discharge cycling process.



ARTICLE INFO

Article history:

Received 25 May 2016

Received in revised form 8 July 2016

Accepted 18 July 2016

Available online 19 July 2016

Keywords:

Nitrogen doping

CoMnO_x

One-dimensional

Lithium ion batteries

ABSTRACT

A novel one-dimensional $\text{CoMnO}_x/\text{N-CNT}$ composite was synthesized by binding Mn-Co nanoparticles on nitrogen doped carbon nanotubes (N-CNT) through solvothermal method and followed by high temperature pyrolysis. The as-made Mn-Co/N-CNT as LIBs anode material exhibits excellent rechargeable capability, i.e. $1028 \text{ mAh}\cdot\text{g}^{-1}$ at $200 \text{ mA}\cdot\text{g}^{-1}$. Doped nitrogen on CNT effectively increase the conductivity of the complex and the binding energy between Mn-Co nanoparticles and CNT, which lead to more stable and higher conductive complex during charge/discharge cycling process.

© 2016 Published by Elsevier B.V.

1. Introduction

With the increasing power and energy demand in portable electronic devices and powering electric vehicles in the modern society, improvement of new lithium-ion batteries (LIBs) anode

materials on cycling stability, energy density, rate capability, cost and safety is imperious demand [1–3,38]. Carefully modulation of anode materials is one critical way to develop new generation LIBs [4]. Transition-metal oxides (TMOs), such as TiO_2 , Co_xO_y , Fe_xO_y , and Mn_3O_4 have been widely investigated as candidates to replace conventional commercial graphite-based anode materials due to their high theoretical capacities and charming reaction mechanism [5–8,33,36].

^{*} Corresponding authors.

Recently, multi transition metal oxides (MTMO) from combination of two transition metal oxides, like CoMn_2O_4 , MnCo_2O_4 , ZnMn_2O_4 , ZnCo_2O_4 etc., are attracting more attention because of their lower cost, higher electronic conductivity and better electrochemical performance compared to single metal oxides [9,31]. Among them, the electrochemical performance of $\text{Co}_x\text{Mn}_{3-x}\text{O}_4$ is outstanding, which could be attributed to the complementarity and synergy the advantage of Co-based and Mn-based metal oxides in the charge/discharge process [10,30]. For example, Lou and co-worker synthesized the double-shelled MnCo_2O_4 hollow microcubes, which deliver a capacity of $624 \text{ mAh}\cdot\text{g}^{-1}$ at a current density of $200 \text{ mA}\cdot\text{g}^{-1}$ after 50 cycles [11]. Despite the great promise of MTMO electrode, two main technical challenges must be addressed before they can find practical use. First, the electronic conductivity of MTMO is still too low in comparison with carbon-based materials. Second, MTMO electrode suffering a large volume change and dramatic mechanical stress during cycling processes, producing a rapid capacity fading and a short cycle life [9,12,13]. As is well known, the microstructure of electrode material is one of the most significant factors to affect its performance [5]. In order to further improve the cycle life of MTMOs, one successful strategy is the combination MTMOs with carbon materials, which could be considered as the conductive and elastic matrix to prevent the exfoliation and agglomeration of MTMOs during rechargeable cycling as well as increase the electrical conductivity of electrode [14,15,34].

Carbon nanotube (CNTs)/TMOs composites for LIB anodes have received increasing interest in recent years because of the excellent conductivity and strong mechanical/chemical stability of CNTs [4]. Such composites were usually combined by chemical interactions between oxygen-containing functional groups of CNTs and the metal oxides. However, the functional oxygen-containing groups of carbonaceous materials either lower the overall electronic conductivity or are not permanently bound with metal oxides, which could cause the peeling of metal oxides and a poor cycle performance [16,17,35]. Previous reports have demonstrated the successful coupling of TMOs with doped heteroatom (e.g., N) carbon-based material to improve the cycle life and the capacity retention of electrode materials [18,32]. The electron-rich nature of dopant atoms can create localized highly reactive sites to accelerate the charge transfer, improving the reaction kinetics and enhancing the interaction force between metal oxides and carbon surface via strong chemical bonding [16]. Inspired by these results, and after comprehensively considering the advantage of MTMOs and N-doped CNTs (NCNT), it is highly interesting to synthesize NCNT/MTMOs hybrid materials for high performance LIBs. However, it remains a challenge to synthesize such hybridize materials through one-pot facile method.

Here in this paper, non-stoichiometric CoMnO_x nanocrystals (named as Mn-Co) have been well dispersed on N-doped CNTs through one-step solvothermal method and followed by high temperature pyrolysis. As an anode material for Li-ion batteries (LIBs), this composite exhibited excellent long-term cycling stability ($608.3 \text{ mAh}\cdot\text{g}^{-1}$ at $2000 \text{ mA}\cdot\text{g}^{-1}$ after 200 cycles) and satisfactory rate capability ($403.3 \text{ mAh}\cdot\text{g}^{-1}$ at $6400 \text{ mA}\cdot\text{g}^{-1}$).

2. Experimental

2.1. Materials preparation

2.1.1. Synthesis of the N-doped CNT/Mn-Co nanohybrids and CNT/Mn-Co nanohybrids

Nitric acid treated CNT was first prepared by nitric acid [28]. For the growth of Mn-Co precursor on the surface of CNT, 100 mg treated CNTs were first dispersed in 40 mL deionized (DI) water by

ultrasonic vibration for 3 h in a capped bottle. Then, 1 mmol KMnO_4 , 1 mmol $\text{CoSO}_4\cdot 7\text{H}_2\text{O}$ and 100 mg dicyandiamide were added into the above suspension and the mixture was stirred by magnetic bar for 30 min. After thorough mixing, the mixture was transferred into Teflon-lined stainless steel autoclave and kept at 120°C for 5 h. After cooling to room temperature, the N-doped CNT/Mn-Co precursor was collected by centrifugation, and washed with deionized water and ethanol for three times and dried in oven. Finally, the N-doped CNT/Mn-Co nanostructure was obtained by calcining the precursor at 500°C for 2 h under an argon atmosphere.

CNT/Mn-Co nanohybrids was prepared as a control sample. For the preparation of this material, CNTs nanotubes are decorated by Mn and Co oxides through the same processes as mentioned above except the introduction of dicyandiamide during hydrothermal treatment.

2.2. Sample characterization

X-ray powder diffraction (XRD) analysis was recorded on X'Pert PRO MPD (Holland) with $\text{Cu K}\alpha$ radiation from 20 to 70° to determine the phase purity and crystal structure of the samples. The surface morphology and microstructure of obtained samples were investigated by field emission scanning electron microscopy (SEM) (HitachiS-4800, Japan) and Transmission electron microscopy (TEM, JEM-2100UHR, Japan). The element content and distribution of the samples were characterized by energy dispersive X-ray spectroscopy (EDS). The Raman spectra were measured on a Renishaw DXR Raman spectros system with a 532 nm laser source, and the spectrum range was from 45 cm^{-1} to 4000 cm^{-1} . The elemental valences and functional groups of the samples were analysed by using X-ray photoelectron spectroscopy (XPS, Thermo Scientific ESCALab250Xi). The contents of Mn-Co MTMO in samples were quantitatively determined by thermogravimetric analysis (TGA, STA 409 PC Luxx, Germany). The specific surface area and the pore structure of the samples were examined by nitrogen adsorption/desorption isotherms using automatic specific surface area measuring equipment (ASAP 2020, America).

2.3. Electrochemical measurement

For preparing working electrodes, a mixture of as-prepared samples, carbon black and poly(vinylidene) fluoride (PVDF) binder at a weight ratio of 80:10:10 was pasted on copper foil current collector. After coating, the prepared working electrode was dried at 100°C in vacuum oven for 10 h to remove any solvent. The electrodes were cut into disks typically with a diameter of $\sim 12 \text{ mm}$, and the average mass of the active materials loading within the coin cells is around 1.2 mg for CNT/Mn-Co and 1.0 mg for CNT/Mn-Co, respectively. Lithium foil was used as the counter electrode and the reference electrode. The electrolyte consisted of a solution 1 mol L^{-1} LiPF_6 in a mixture of dimethyl carbonate (DMC) and ethylene carbonate (EC) (1:1, in wt.%) obtained from MTI Corporation. The galvanostatic method at the different charge/discharge current densities from $0.1 \text{ A}\cdot\text{g}^{-1}$ to $6.4 \text{ A}\cdot\text{g}^{-1}$ was employed to measure the electrochemical capacity and cycle life of the electrode at room temperature using a LAND-CT2001A cycler. Cyclic voltammograms (CV) were performed using an Ametek PARSTAT4000 electrochemistry workstation at 0.2 mV s^{-1} within the potential range of 0.01–3.0 V. Electrochemical impedance spectra (EIS) was performed using an Ametek PARSTAT4000 electrochemistry workstation in the frequency range of 100 kHz to 10 mHz with AC voltage amplitude of 10 mV.

3. Results and discussion

3.1. Structural characterization

The synthesis strategy of N-doped CNT/Mn-Co nanohybrids (NCNT/Mn-Co) was illustrated in Fig. 1. In the first, CNT was pretreated by nitric acid [28]. Then, the modified CNTs were mixed with another aqueous solution (containing certain amount KMnO_4 , $\text{CoSO}_4 \cdot 7\text{H}_2\text{O}$ and dicyandiamide) and sealed into an autoclave to heat at 120°C for 5 h. Two reactions occurred in the hydrothermal process: (i) irregular MnO_x -precursor was formed on the surface of CNTs via the redox reaction between KMnO_4 and CNTs, and Co^{2+} ions were simultaneously incorporated into the lattice of MnO_x to form the Co doped MnO_x precursor [19]. (ii) Dicyandiamide was combined with CNTs via nucleophilic reaction between the amino groups of dicyandiamide and the oxygen-containing groups on CNTs. Afterwards, the as-obtained NCNT/Mn-Co precursor was calcination at 500°C to induce the formation of NCNT/Mn-Co nanohybrids. To further understand the function of N doping, CNT/Mn-Co nanohybrids was prepared as contrast sample. During the preparation of CNT/Mn-Co, CNTs nanotubes were decorated by Mn and Co oxides through the same processes as mentioned above except the introduction of dicyandiamide in hydrothermal treatment.

The structural characteristics of CNT/Mn-Co and NCNT/Mn-Co nanohybrids were determined by X-ray powder diffraction (XRD), as shown in Fig. 2a. The diffraction peaks at 35.6° and 40.6° correspond well to the (1 1 0) and (1 1 3) planes of hexagonal Mn_2O_3 (JCPDS card No. 33-0900), while 36.0° and 60.0° can be assigned to (2 1 1) and (2 2 4) reflections of tetragonal Mn_3O_4 (JCPDS card No. 18-0803). It should be noted that the signals originating from cobalt-containing species were ambiguous, and the reasons may be due to the complete incorporation of Co into lattice of manganese oxide [19]. The broad and weak peaks indicated the crystallinity of the Mn-Co MTMO was low and the crystallized size was small [5].

The microstructural of as-prepared samples was investigated by SEM and TEM. The panoramic view of CNT/Mn-Co and NCNT/Mn-Co by SEM reveals that Mn-Co nanoparticles uniformly decorated on the entire surface of CNTs and the size of Mn-Co for NCNT/Mn-Co sample is somewhat smaller than that for CNT/Mn-Co sample (Fig. S1). In the TEM image of NCNT/Mn-Co nanohybrids (Fig. 3b and Fig. S2a), the nanocrystals of Mn-Co were well dispersed in the surface of CNTs, and the average size of Mn-Co is about 18 nm, which is somewhat smaller than that in CNT/Mn-Co nanohybrids (around 26 nm, Fig. 3a and Fig. S2b). No self-congestion nanoparticles were observed either in CNT/Mn-Co and NCNT/Mn-Co nanohybrids, indicated binding energy between Mn-Co and per-treated CNT were stronger than Mn-Co themselves.

High-resolution (HR) TEM image of NCNT/Mn-Co nanohybrids was presented in Fig. 3b, and the lattice fringes of Mn-Co could be easily identified (inset Fig. 3b). The measured interplanar spacing of 0.21 nm in Fig. 3b indexed to the d -spacing of the (1 1 3) plane of tetragonal CoMn_2O_4 crystals [29]. The EDS elemental mapping of a single NCNT/Mn-Co nanohybrids was shown in Fig. 3c, unambiguously confirming the uniform distribution of Mn and Co elements in the Mn-Co nanoparticles. Besides, the most N atoms were well and continually dispersed on the surface of CNT in the right of Fig. 3c, even at the domains that binding with Mn-Co nanocrystals, which indicated that the N source possess higher reactivity or stronger interaction with per-treated CNT than Mn-Co nanocrystals. As the result, the nanoparticles that packing on N-doped CNT were smaller and denser than that on bare CNT. The EDS data (Fig. S3) revealed the ratio of Mn and Co in NCNT/Mn-Co nanohybrids was 10.58 at.% and 7.84 at.%, respectively.

Fig. 2b shows the Raman spectra of CNT/Mn-Co and NCNT/Mn-Co nanohybrids, which contained two strong characteristic peaks at 1350 cm^{-1} and 1590 cm^{-1} in both samples. The D band at 1350 cm^{-1} could be ascribed to structural defects or amorphous carbon, while G band at 1590 cm^{-1} corresponded to the π - π stacking of conjugated carbons in the mixture [20]. The I_D/I_G ratio for NCNT/Mn-Co nanohybrids (0.97) was greater than CNT/Mn-Co nanohybrids (0.87), demonstrating the successful doped nitrogen atoms in NCNT/Mn-Co samples [21,23].

To investigate the chemical composition and the atoms valence states of the NCNT/Mn-Co nanohybrids, X-ray Photoelectron Spectroscopy (XPS) spectra were tested, as shown in Fig. 4 and Fig. S4. The spectrum was normalized for any background signals using the Shirley algorithm [22]. The characteristic peaks of Mn, Co, O, C and N atoms could be obviously identified in full XPS spectra of the composite (Fig. S4a). The N 1s spectrum can be deconvoluted into three components, centered at 398.6 eV (N-6, pyridinic N, 44.2%), 399.8 eV (N-5, pyrrolic N, 32.1%) and 401.3 eV (N-4, quaternary N, 23.7%), respectively, which ascribed to the nucleophile substitution reaction of dicyandiamide and pretreated CNT matrix [23,37]. The N content of NCNT/Mn-Co nanohybrids is calculated to be $\sim 4.0\%$. The high N-containing rate (especially, N-5 and N-6, Table S1) affords more electrochemically active sites during lithium storages. Additionally, the N-containing groups could be considered as “bridge” to enhance the binding energy between Mn-Co and CNT, both of which were beneficial for enhancing electrochemical performances of NCNT/Mn-Co. The oxygen-containing groups of NCNT/Mn-Co nanohybrids is obviously lower than that in CNT/Mn-Co nanohybrids (Fig. S4c), indicating NCNT/Mn-Co has higher electrical conductivity [21]. The high resolution C 1s spectrum (Fig. 4b) was centered at 284.7 eV, which could be well identified into three components at binding energies of 284.5 eV

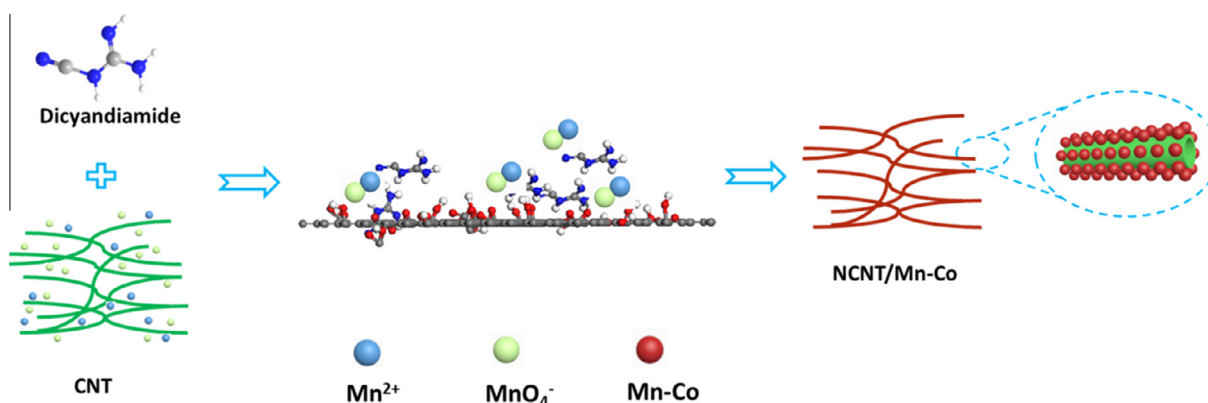


Fig. 1. Schematic illustration of the formation of NCNT/Mn-Co nanohybrids.

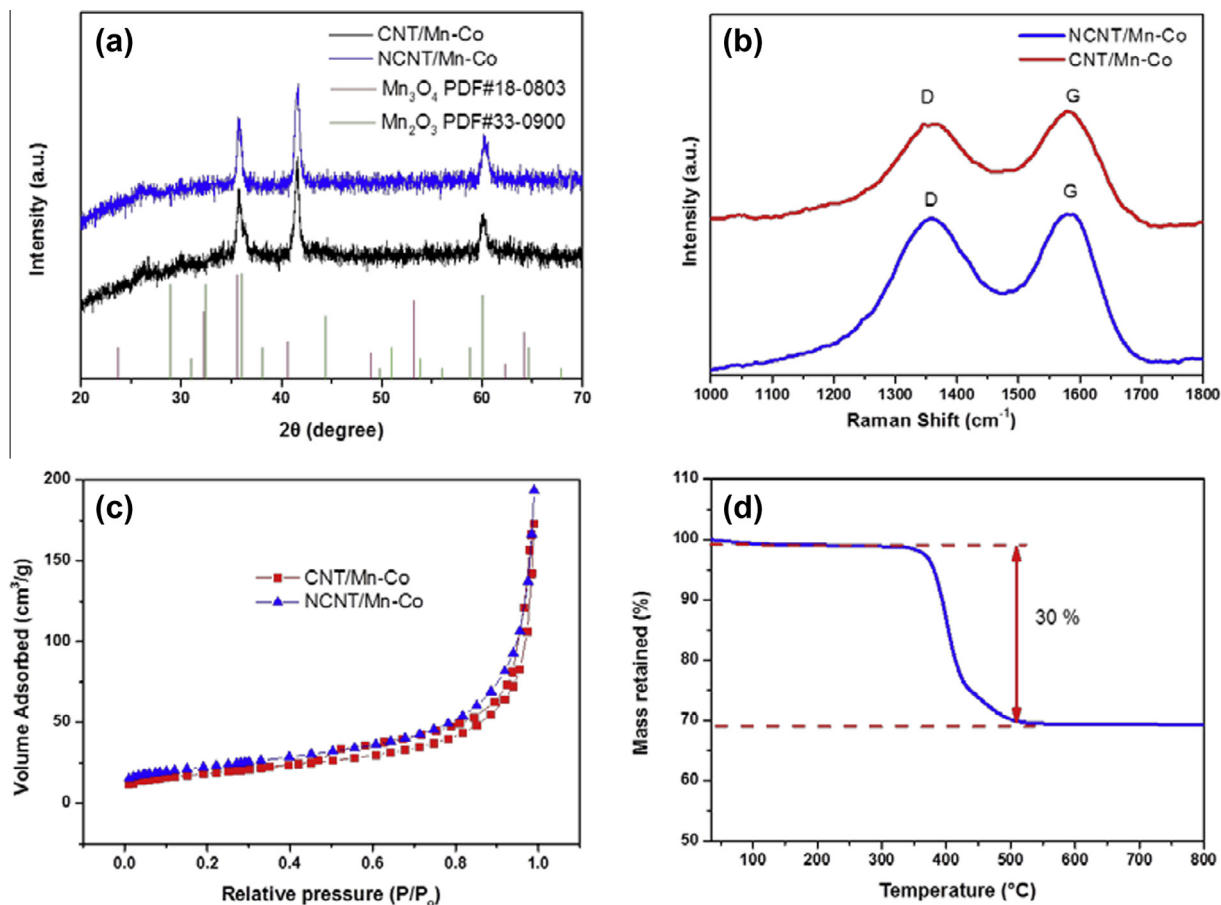


Fig. 2. (a) XRD patterns of as-prepared CNT/Mn-Co and NCNT/Mn-Co nanohybrids, (b) Raman spectrum of CNT/Mn-Co and NCNT/Mn-Co nanohybrids, (c) N₂ adsorption and desorption isotherms of CNT/Mn-Co and NCNT/Mn-Co nanohybrids, (d) TGA curve of NCNT/Mn-Co nanohybrids in air.

(C–C/C=C), 285.1 eV (C–N), and 285.9 eV (C–O), respectively [18,24]. It could be easily identified that there was an obviously decrease in the epoxy group content after N doping (Fig. 4b and Fig. S4c). Furthermore, the imino group content was considerably increased, which ascribed to the nucleophile substitution reaction of dicyandiamide and CNT. The content of graphitic carbon in NCNT/Mn-Co nanohybrids was obviously increased due to the N doping, which provided feasible pathways for Li⁺ penetration and charge transfer. The Mn 2p spectrum featured two main peaks entered at 642.0 eV and 653.5 eV respectively, and the spin energy separation of Mn 2p_{3/2} and Mn 2p_{1/2} was 11.5 eV, which were in good agreement with reported data in CoMn₂O₄ (Fig. 4c) [25]. After refined fitting, the spectrum could be deconvoluted into four peaks at binding energies of 641.5 eV (Mn²⁺), 642.9 eV (Mn³⁺), 653.1 eV (Mn²⁺), and 653.7 eV (Mn³⁺), respectively. The Co 2p XPS spectra of NCNT/Mn-Co nanohybrids exhibited two characteristic peaks (795.6 and 780.2 eV), corresponding to the Co 2p_{1/2} and Co 2p_{3/2} spin-orbit peaks of Co²⁺ (Fig. 4d) [26]. The other two minor peaks at 802.9 eV and 786.3 eV were associated with satellite peaks. Therefore, it was reasonable to conclude that the solid-state redox couples of Mn³⁺/Mn²⁺ and Co³⁺/Co²⁺ exists in NCNT/Mn-Co samples, which may exhibit higher electrical conductivity and electrochemical activity due to the synergetic effects of multiple valences of the cations [9].

The N₂ adsorption isotherms for the as-prepared samples were shown in Fig. S5. Both isotherm curves has a representative H3-type N₂ adsorption-desorption hysteresis (Fig. 2c). The BET surface of the NCNT/Mn-Co nanohybrids was 79.12 m²g⁻¹, larger than that of CNT/Mn-Co nanohybrids (64.97 m²g⁻¹) (Table S2). The N doping

significantly increased the roughness of the system, which can be ascribed to the in situ grown of g-CN_x nanostructure on the surface of CNT and well dispersed smaller MTMO nanoparticles (also have been approved by TEM data). The thermal properties and the compositions of NCNT/Mn-Co nanohybrids were analyzed by TGA. As shown in Fig. 2d, the major mass loss occurred in the range of 350–500 °C, which could be ascribed to the combustion of organic in air. Therefore, we could deduce that the content of Mn-Co in NCNT/Mn-Co was about 70%.

3.2. Electrochemical characterization

Fig. 5a showed the first galvanostatic discharge-charge profiles of the CNT/Mn-Co and NCNT/Mn-Co nanohybrids at a current density of 200 mA·g⁻¹ between 0.01 and 3.0 V. The NCNT/Mn-Co nanohybrids showed greatly improved electrochemical performance with higher initial discharge-charge capacities (1589 and 1052 mAh·g⁻¹) and coulombic efficiency (66.2%) than that of CNT/Mn-Co nanohybrids (1409 and 901 mAh·g⁻¹, 63.9%). The higher initial discharge-charge capacities could be ascribed to the smaller Mn-Co nanoparticles in NCNT/Mn-Co [21]. The initial capacity loss could be attributed to the formation of SEI layer and the incomplete extraction of lithium from the active material, which represented a bunch of uncontrollable side reaction that contributes to a large irreversible capacity [10,11,25]. To further study the mechanism of lithium storage during charge-discharge cycles, cyclic voltammetry of CNT/Mn-Co nanohybrids was given in Fig. 5b. During the discharge process in the first cycle, two pronounced cathodic peaks at 0.5 V and 0.25 V were observed, corre-

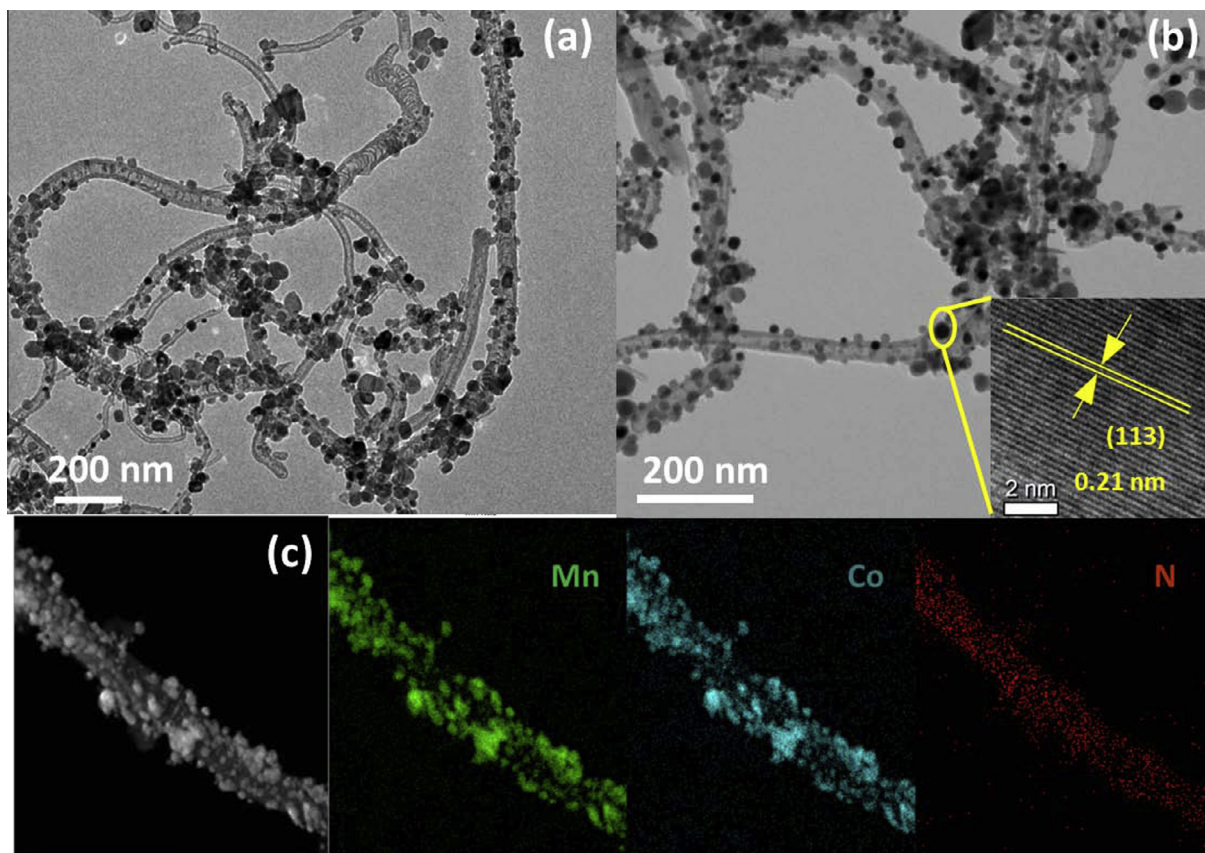


Fig. 3. TEM images of (a) CNT/Mn-Co and (b) NCNT/Mn-Co nanohybrids. (c) Color EDS mapping images of one single NCNT/Mn-Co nanohybrids. The inset of (b) shows a HRTEM image of Mn-Co nanohybrids. (For interpretation of the references to colour in this figure legend, the reader is referred to the web version of this article.)

sponding to the formation of metallic Mn and Co from MnO_x and CoO_x , respectively [11,26]. There were two oxidation peaks at 1.45 V and 2.0 V could be observed in the following anodic sweep, which could be assigned to the formation of MnO_x and CoO_x from metallic Mn and Co [19]. From the second cycle onward, the reduction peak at 0.25 V disappeared and the peak at 0.5 V and 2.0 V were slightly shifted to higher potential (0.51 V for cathodic peak and 2.05 V for anodic peak). The slight higher cathodic/anodic potential could reduce the electrode polarization and improve the charge transfer kinetics, which means the reduction and oxidation becomes more easies in the subsequent cycles after the activation in the first cycle [27]. Besides, a reversible, broad but discriminable reduction peak that centered at about 0.9 V had appeared ever since the second cycle, which also could be observed in many previous reports [10,25]. The almost overlap CV curves of the second and fifth cycles indicated highly reversible redox behavior and good cycling stability of NCNT/Mn-Co nanohybrids, similar results could also be observed in the discharge-charge voltage profiles (Fig. S5).

Fig. 6a shows long time cycling performance of CNT/Mn-Co and NCNT/Mn-Co nanohybrids at a current density of 200 mA g^{-1} between 3.0 and 0.01 V. As shown, the discharge capacity of the NCNT/Mn-Co electrode was around 1011 mAh g^{-1} in the second, and the capacity was 1028 mAh g^{-1} after 100 cycles with nearly 100% coulombic efficiency. As a comparison, the discharge capacity of CNT/Mn-Co electrode at second cycle was 1007 mAh g^{-1} , and it attenuated quickly to 450 mAh g^{-1} after 50 cycles. The poor cycling stability of CNT/Mn-Co electrodes are due to the tremendous volume changes of Mn-Co nanoparticles, results to electrode disintegration. Remarkably, even at a high current density of 2.0 A g^{-1} , the CNT/Mn-Co nanohybrids still shows excellent long-cyclic

performance with higher capacity (608 mAh g^{-1}) and retention (82.5%) than that of CNT/Mn-Co electrode (296 mAh g^{-1} , 51.7%) after 200 cycles (Fig. 6b). More importantly, the discharge capacity of NCNT/Mn-Co electrode could still up to 500 mAh g^{-1} even after 360 cycles at such high current density (Fig. S6).

The remarkable improved stability could be attributed to the introduction of nitrogen atoms on the CNT, which not only increased binding energy between MTMO and CNT to reach a high stable nanostructure, but also played as surfactant to form smaller and well-dispersed MTMO nanoparticles on CNT to facile Li^+ penetration and charges transfer. As expected, NCNT/Mn-Co electrode also indicated remarkable rate performance and reversible capacity, as shown in Fig. 6c. The average discharge capacities of the NCNT/Mn-Co electrode at 100 mA g^{-1} , 200 mA g^{-1} , 400 mA g^{-1} , 800 mA g^{-1} , 1600 mA g^{-1} , 3200 mA g^{-1} and 6400 mA g^{-1} were 1196 mAh g^{-1} , 1119 mAh g^{-1} , 1022 mAh g^{-1} , 956 mAh g^{-1} , 854 mAh g^{-1} , 656 mAh g^{-1} , and 435 mAh g^{-1} , respectively, which are much better than those of CNT/Mn-Co anodes. When the current density was reduced backed to 100 mA g^{-1} , a specific capacity of 1324 mAh g^{-1} could be restored, which indicated the excellent robustness and stability of NCNT/Mn-Co nanohybrids even after high rate long time cycling.

In order to further understand the lithium storage capability of NCNT/Mn-Co nanohybrids, electrochemical impedance measurements were carried out. Fig. 6d showed the Nyquist plots of the CNT/Mn-Co and NCNT/Mn-Co electrodes at the open-circuit voltage before cycling. The high-medium frequency region at the real axis corresponded to the ohmic resistance (R_s) and the charge transfer resistance (R_{ct}) at the interface, and an inclined line located in the low frequency region represents the diffusion resistance. Compared with CNT/Mn-Co electrode, NCNT/Mn-Co elec-

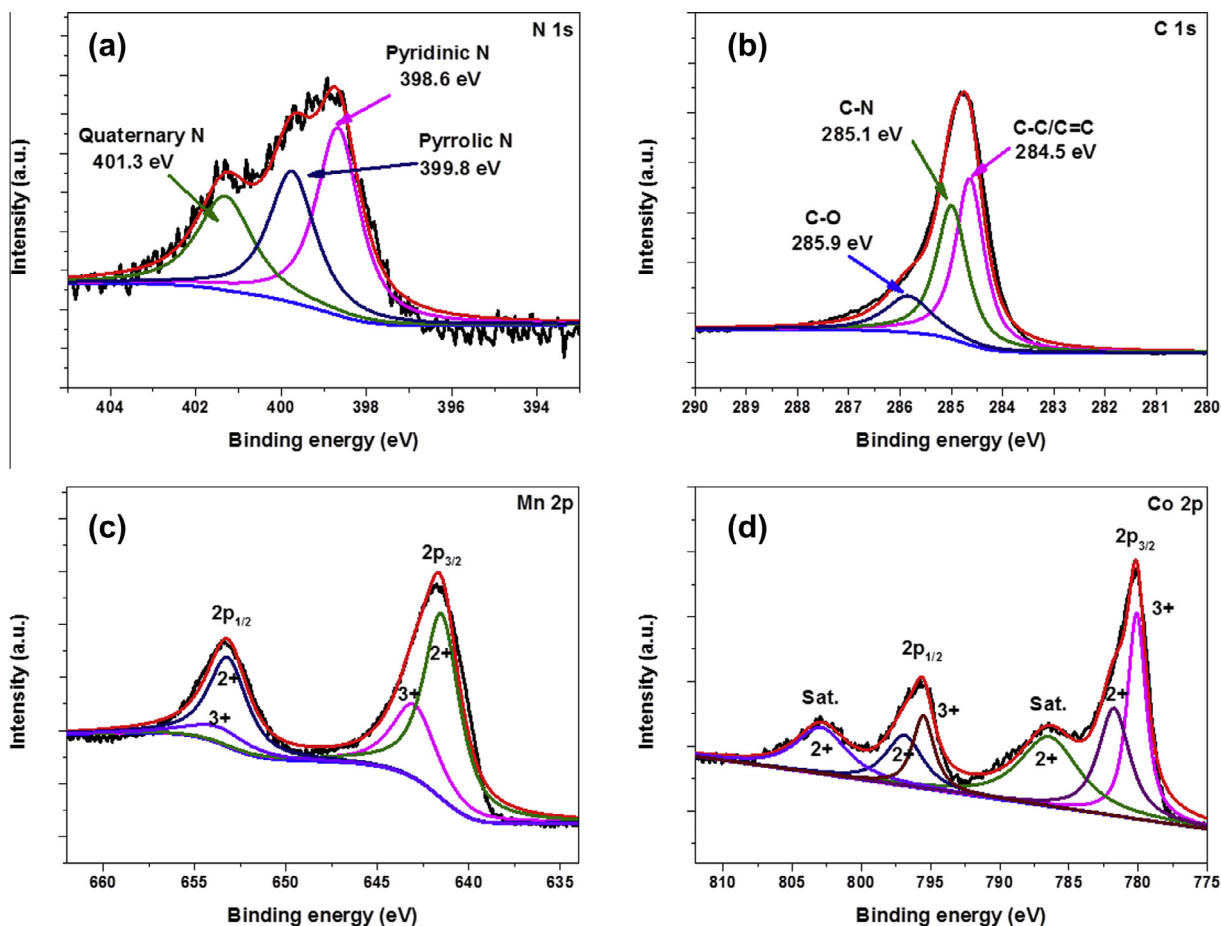


Fig. 4. XPS spectra of (a) N 1s, (b) C 1s, (c) Mn 2p, and (d) Co 2p regions of NCNT/Mn-Co nano hybrids.

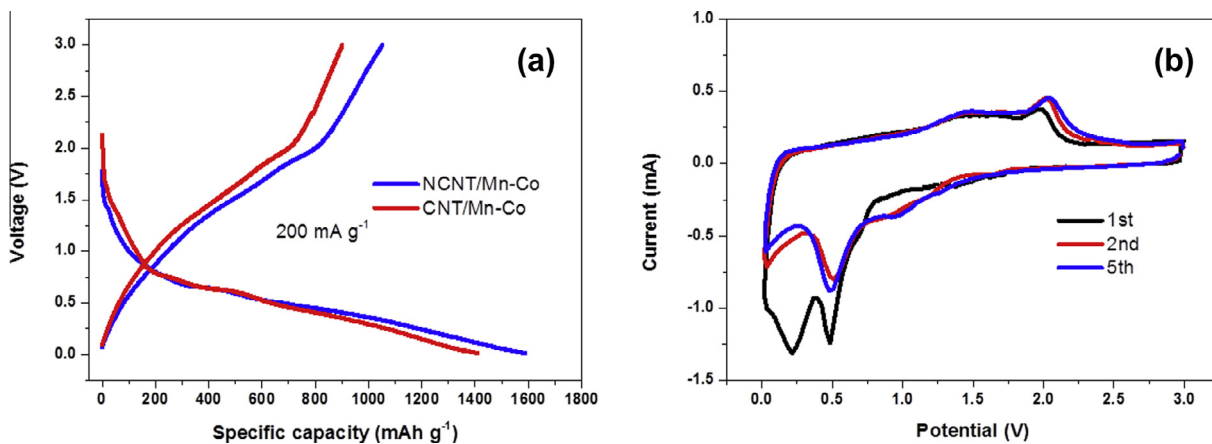


Fig. 5. (a) Discharge-charge profiles of CNT/Mn-Co and NCNT/Mn-Co nano hybrids electrode at a constant current density of 200 mA g^{-1} , (b) CV curves of NCNT/Mn-Co anode at 0.2 mV s^{-1} scanning rate.

trode exhibits a smaller semicircle diameter, reflected a lower electrical resistance. More important, the charge transfer resistance of the CNT/Mn-Co is almost unchanged after 20 cycles (Fig. S7). However, for CNT/Mn-Co electrode, the semicircle diameter was significantly increased. The different behaviors of CNT/Mn-Co and NCNT/Mn-Co electrodes further indicate that the introduction of dicyandiamide can not only improve the electrical conductivity of materials, but also improve the stability of the material.

All in all, NCNT/Mn-Co nano hybrids present outstanding electrochemical properties, which could be attributed to the following reasons. Firstly, the N-doping on CNT matrix by dicyandiamide through chemical bonding introduced a great number of active nitrile groupings and fixed the defects on CNTs and the interspace between CNTs and MTMO NPs to achieve higher electrical conductivity and increase the compatibility with electrolyte, which leads to greatly improved rate performance. Secondly, the involvement

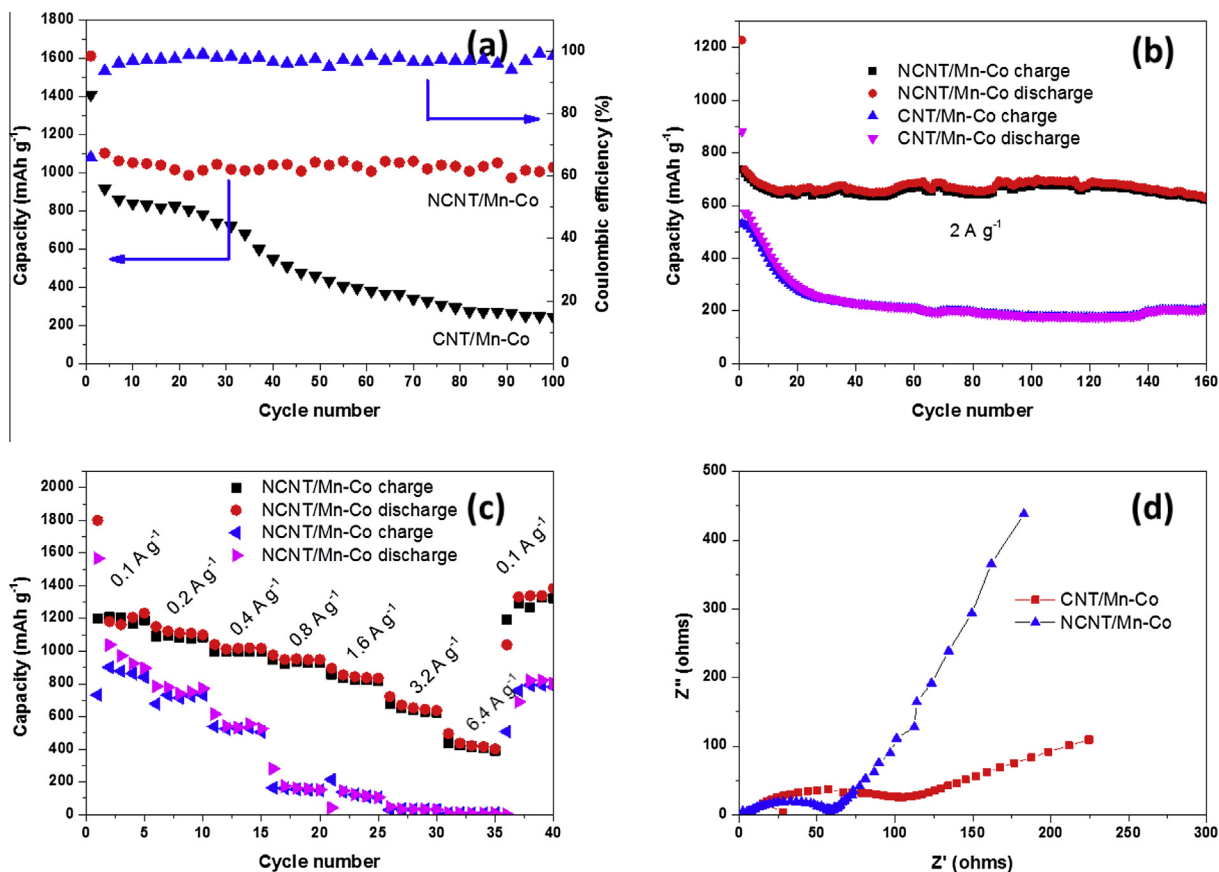


Fig. 6. (a) Cycling performance and Coulombic efficiency of the NCNT/Mn-Co electrodes at 0.2 A g^{-1} for 100 cycles. (b) Discharge-charge capacities of CNT/Mn-Co and NCNT/Mn-Co electrodes at a current density of 2 A g^{-1} . (c) Rate performance of NCNT/Mn-Co and CNT/Mn-Co electrodes at different current densities. (d) electrochemical impedance spectra of CNT/Mn-Co and NCNT/Mn-Co electrodes before cycles.

of dicyandiamide as nitrogen source could effectively reduce the size of MTMO NPs, which can be more uniformly dispersed on the doped CNT. Through facilitating the lithium ions and charges transfer of the structure, the charge/discharge capacity and rate performance are improved, simultaneously. In the last, dicyandiamide that reacted on CNT surface could be considered as “bridge” between MOTO NPs and CNT, which result in a high-strength flexibility to accommodate the large volume expansion. The structure of NCNT/Mn-Co nanohybrids can be more effectively stabilized by covalent interactions between the two moieties via a C-N bond, preventing the nanoparticles peeling off from the buffering matrixes, demonstrating the excellent cycling stability.

4. Conclusion

In summary, a low cost, readily available Mn-Co/N-CNT composite have been synthesized in a controllable approach as electrode for LIBs. Compared with CNT/Mn-Co nanohybrids, the NCNT/Mn-Co nanohybrids exhibits following advantages: 1. dicyandiamide could be considered as surfactant during metal oxide deposition process, which leads to smaller Mn-Co nanoparticles on CNT through much stronger chemical bonds; 2. the imidization reaction during N-doping could effectively reduce pre-oxidized CNTs to increase the conductivity of composite. As a result, a high rechargeable capacity of 1028 mA g^{-1} for NCNT/Mn-Co nanohybrids could be reached after 100 cycles at the current density of 200 mA g^{-1} . Besides, the rate capability of NCNT/Mn-Co is obviously improved (434.9 mA g^{-1} at 6.4 A g^{-1}). Therefore, the methodology described here would potentially

afford a way to develop novel anode materials with high rechargeable capacity and rate capability for next generation lithium-ion batteries anode.

Acknowledgements

This work is supported by the National Natural Science Foundation of China (Nos. 51303212, 21572269, 51303202, 21302224); National Natural Science Foundation of Shandong Province (ZR2013BQ028, ZR2013EMQ013); The Fundamental Research Fund for the Central Universities (14CX02196A, 15CX08005A, 15CX05010A) and Qingdao science and technology plan (15-9-1-108-jch).

Appendix A. Supplementary data

Supplementary data associated with this article can be found, in the online version, at <http://dx.doi.org/10.1016/j.cej.2016.07.071>.

References

- [1] M.V. Reddy, G.V. Subba Rao, B.V.R. Chowdari, Metal oxides and oxysalts as anode materials for Li ion batteries, *Chem. Rev.* 113 (2013) 5364–5457.
- [2] Z. Yang, J. Ren, Z. Zhang, X. Chen, G. Guan, L. Qiu, Y. Zhang, H. Peng, Recent advancement of nanostructured carbon for energy applications, *Chem. Rev.* 115 (2015) 5159–5223.
- [3] J.S. Chen, X.W. Lou, SnO₂-based nanomaterials: synthesis and application in lithium-ion batteries, *Small* 9 (2013) 1877–1893.
- [4] S. Goriparti, E. Miele, F.D. Angelis, E.D. Fabrizio, R.P. Zaccaria, C. Capiglia, Review on recent progress of nanostructured anode materials for Li-ion batteries, *J. Power Sources* 257 (2014) 421–443.

- [5] Z. Li, Y. Wang, H. Sun, W. Wu, M. Liu, J. Zhou, G. Wu, M. Wu, Synthesis of nanocomposites with carbon-SnO₂ dual-shells on TiO₂ nanotubes and their application in lithium ion batteries, *J. Mater. Chem. A* 3 (2015) 16057–16063.
- [6] X.W. Lou, D. Deng, J.Y. Lee, J. Feng, L.A. Archer, Self-supported formation of needlelike Co₃O₄ nanotubes and their application as lithium-ion battery electrodes, *Adv. Mater.* 20 (2008) 258–262.
- [7] J.S. Cho, Y.J. Hong, Y.C. Kang, Design and synthesis of bubble-nanorod-structured Fe₂O₃ carbon nanofibers as advanced anode material for Li-ion batteries, *ACS Nano* 9 (2015) 4026–4035.
- [8] S.Z. Huang, Y. Cai, J. Jin, J. Liu, Y. Li, Y. Yu, H. Wang, L. Chen, B. Su, Hierarchical mesoporous urchin-like Mn₃O₄/carbon microspheres with highly enhanced lithium battery performance by in-situ carbonization of new lamellar manganese alkoxide (Mn-DEG), *Nano Energy* 12 (2015) 833–844.
- [9] C. Yuan, H.B. Wu, Y. Xie, X.W. Lou, Mixed transition-metal oxides: design, synthesis, and energy-related applications, *Angew. Chem. Int. Ed.* 53 (2014) 1488–1504.
- [10] L. Yu, L. Zhang, H.B. Wu, G. Zhang, X.W. Lou, Controlled synthesis of hierarchical Co_xMn_{3-x}O₄ array micro-/nanostructures with tunable morphology and composition as integrated electrodes for lithium-ion batteries, *Energy Environ. Sci.* 6 (2013) 2664–2671.
- [11] L. Zhou, D. Zhao, X.W. Lou, Double-shelled CoMn₂O₄ hollow microcubes as high-capacity anodes for lithium-ion batteries, *Adv. Mater.* 24 (2012) 745–748.
- [12] Z. Bai, N. Fan, C. Sun, Z. Ju, C. Guo, J. Yang, Y. Qian, Facile synthesis of loaf-like ZnMn₂O₄ nanorods and their excellent performance in Li-ion batteries, *Nanoscale* 5 (2013) 2442–2447.
- [13] J. Bai, X. Li, G. Liu, Y. Qian, S. Xiong, Unusual formation of ZnCo₂O₄ 3D hierarchical twin microspheres as a high-rate and ultralong-life lithium-ion battery anode material, *Adv. Funct. Mater.* 24 (2014) 3012–3020.
- [14] B. Liu, J. Zhang, X. Wang, G. Chen, D. Chen, C. Zhou, G. Shen, Hierarchical three-dimensional ZnCo₂O₄ nanowire arrays/carbon cloth anodes for a novel class of high performance flexible lithium-ion batteries, *Nano Lett.* 12 (2012) 3005–3011.
- [15] B. Liu, X. Wang, B. Liu, Q. Wang, D. Tan, W. Song, X. Hou, D. Chen, G. Shen, Advanced rechargeable lithium-ion batteries based on bendable ZnCo₂O₄-urchins-on-carbon-fibers electrodes, *Nano Res.* 6 (2013) 525–534.
- [16] Y. Hou, J. Li, Z. Wen, S. Cui, C. Yuan, J. Chen, N-doped graphene/porous g-C₃N₄ nanosheets supported layered-MoS₂ hybrid as robust anode materials for lithium-ion batteries, *Nano Energy* 8 (2014) 157–164.
- [17] J.P. Paraknowitsch, A. Thomas, Doping carbons beyond nitrogen: an overview of advanced heteroatom doped carbons with boron, sulphur and phosphorus for energy applications, *Energy Environ. Sci.* 6 (2013) 2839–2855.
- [18] S. Liu, Y. Dong, C. Zhao, Z. Zhao, C. Yu, Z. Wang, J. Qiu, Nitrogen-rich carbon coupled multifunctional metal oxide/graphene nanohybrids for long-life lithium storage and efficient oxygen reduction, *Nano Energy* 12 (2015) 578–587.
- [19] Y. Guo, L. Yu, C. Wang, Z. Lin, X.W. Lou, Hierarchical tubular structures composed of Mn-based mixed metal oxide nanoflakes with enhanced electrochemical properties, *Adv. Funct. Mater.* 25 (2015) 5184–5189.
- [20] Z. Cai, L. Xu, M. Yan, C. Han, L. He, K.M. Hercule, C. Niu, Z. Yuan, W. Xu, L. Qu, K. Zhao, L. Mai, Manganese oxide/carbon yolk-shell nanorod anodes for high capacity lithium batteries, *Nano Lett.* 15 (2015) 738–744.
- [21] Z. Li, G. Wu, S. Deng, S. Wang, Y. Wang, J. Zhou, S. Wu, W. Wu, M. Wu, Combination of uniform SnO₂ nanocrystals with nitrogen doped graphene for high-performance lithium-ion batteries anode, *Chem. Eng. J.* 283 (2016) 1435–1442.
- [22] D.A. Shirley, High-resolution X-ray photoemission spectrum of the valence bands of gold, *J. Phys. Rev.* 5 (1972) 4709–4714.
- [23] F. Zheng, Y. Yang, Q. Chen, High lithium anodic performance of highly nitrogen-doped porous carbon prepared from a metal-organic framework, *Nat. Commun.* 5 (2014) 5261–5271.
- [24] S. Liu, Y. Dong, Z. Wang, H. Huang, Z. Zhao, J. Qiu, Towards efficient electrocatalysts for oxygen reduction by doping cobalt into graphene-supported graphitic carbon nitride, *J. Mater. Chem.* 3 (2015) 19657–19661.
- [25] J. Li, S. Xiong, X. Li, Y. Qian, A facile route to synthesize multiporous MnCo₂O₄ and CoMn₂O₄ spinel quasi-hollow spheres with improved lithium storage properties, *Nanoscale* 5 (2013) 2045–2054.
- [26] Z. Wu, W. Ren, L. Wen, L. Gao, J. Zhao, Z. Chen, G. Zhou, F. Li, H. Cheng, Graphene anchored with Co₃O₄ nanoparticles as anode of lithium ion batteries with enhanced reversible capacity and cyclic performance, *ACS Nano* 6 (2010) 3187–3194.
- [27] N. Wang, J. Yue, L. Chen, Y. Qian, J. Yang, Hydrogenated TiO₂ branches coated Mn₃O₄ nanorods as an advanced anode material for lithium ion batteries, *ACS Appl. Mater. Interfaces* 7 (2015) 10348–10355.
- [28] Z. Wang, D. Luan, S. Madhavi, Y. Hu, X.W. Lou, Assembling carbon-coated α-Fe₂O₃ hollow nanohorns on the CNT backbone for superior lithium storage capability, *Energy Environ. Sci.* 5 (2012) 5252–5256.
- [29] S. Peng, L. Li, Y. Hu, M. Srinivasan, F. Cheng, J. Chen, S. Ramakrishna, Fabrication of spinel one-dimensional architectures by single-spinneret electrospinning for energy storage applications, *ACS Nano* 9 (2015) 1945–1954.
- [30] C. Fu, G. Li, D. Luo, X. Huang, J. Zheng, L. Li, One-step calcination-free synthesis of multicomponent spinel assembled microspheres for high-performance anodes of Li-ion batteries: a case study of MnCo₂O₄, *ACS Appl. Mater. Interfaces* 6 (2014) 2439–2449.
- [31] Z. Zhang, Y. Ji, J. Li, Q. Tan, Z. Zhong, F. Su, Yolk shell Mn_xCo_{1-x}Fe₂O₄ hollow microspheres and their embedded form in carbon for highly reversible lithium storage, *ACS Appl. Mater. Interfaces* 7 (2015) 6300–6309.
- [32] Y. Liu, X. Wang, Y. Dong, Z. Wang, Z. Zhao, J. Qiu, Nitrogen-doped graphene nanoribbons for high-performance lithium ion batteries, *J. Mater. Chem.* 2 (2014) 16832–16835.
- [33] S. Liu, Y. Wang, Y. Dong, Z. Zhao, Z. Wang, J. Qiu, Ultrafine Fe₃O₄ quantum dots on hybrid carbon nanosheets for long-life, high-rate alkali-metal storage, *ChemElectroChem* 3 (2016) 38–44.
- [34] H. Hu, Z. Zhao, W. Wan, Y. Gogotsi, J. Qiu, Polymer/graphene hybrid aerogel with high compressibility, conductivity, and “sticky” superhydrophobicity, *ACS Appl. Mater. Interfaces* 6 (2015) 3242–3249.
- [35] Y. Dong, Z. Zhao, Z. Wang, Y. Liu, X. Wang, J. Qiu, Dually fixed SnO₂ nanoparticles on graphene nanosheets by polyaniline coating for superior lithium storage, *ACS Appl. Mater. Interfaces* 7 (2015) 2444–2451.
- [36] Y. Dong, S. Liu, Z. Wang, Y. Liu, Z. Zhao, J. Qiu, Compressible graphene aerogel supported CoO nanostructures as a binder-free electrode for high-performance lithium-ion batteries, *RSC Adv.* 5 (2015) 8929–8932.
- [37] Y. Liu, X. Wang, W. Wan, L. Li, Y. Dong, Z. Zhao, J. Qiu, Multifunctional nitrogen-doped graphene nanoribbon aerogels for superior lithium storage and cell culture, *Nanoscale* 8 (2016) 2159–2167.
- [38] Y. Dong, S. Liu, Z. Wang, Y. Liu, Z. Zhao, J. Qiu, Sulfur-infiltrated graphene-backed mesoporous carbon nanosheets with a conductive polymer coating for long-life lithium-sulfur batteries, *Nanoscale* 7 (2015) 7569–7573.